










Route to form skyrmions in soft magnetic films

Cite as: APL Mater. 7, 081114 (2019); <https://doi.org/10.1063/1.5093371>

Submitted: 20 February 2019 . Accepted: 28 July 2019 . Published Online: 16 August 2019

D. Navas , R. V. Verba , A. Hierro-Rodriguez , S. A. Bunyaev , X. Zhou, A. O. Adeyeye , O. V. Dobrovolskiy , B. A. Ivanov , K. Y. Guslienko , and G. N. Kakazei 



View Online



Export Citation



CrossMark

ARTICLES YOU MAY BE INTERESTED IN

Perspective: Magnetic skyrmions—Overview of recent progress in an active research field
Journal of Applied Physics **124**, 240901 (2018); <https://doi.org/10.1063/1.5048972>

The design and verification of MuMax3

AIP Advances **4**, 107133 (2014); <https://doi.org/10.1063/1.4899186>

Opportunities and challenges for magnetoelectric devices

APL Materials **7**, 080905 (2019); <https://doi.org/10.1063/1.5112089>



Measure Ready
M91 FastHall™ Controller

A revolutionary new instrument
for complete Hall analysis

See the video 

Lake Shore
CRYOTRONICS

Route to form skyrmions in soft magnetic films

Cite as: APL Mater. 7, 081114 (2019); doi: 10.1063/1.5093371

Submitted: 20 February 2019 • Accepted: 28 July 2019 •

Published Online: 16 August 2019



D. Navas,¹  R. V. Verba,²  A. Hierro-Rodriguez,^{1,3}  S. A. Bunyaev,¹  X. Zhou,⁴  A. O. Adeyeye,⁴ 
O. V. Dobrovolskiy,^{5,6}  B. A. Ivanov,^{2,7}  K. Y. Guslienko,^{8,9}  and G. N. Kakazei^{1,a)} 

AFFILIATIONS

¹Institute of Physics for Advanced Materials, Nanotechnology and Photonics (IFIMUP)/Departamento de Física e Astronomia, Universidade do Porto, 4169-007 Porto, Portugal

²Institute of Magnetism, National Academy of Sciences of Ukraine, 03142 Kyiv, Ukraine

³School of Physics and Astronomy, University of Glasgow, G12 8QQ Glasgow, United Kingdom

⁴Department of Electrical and Computer Engineering, National University of Singapore, 117583, Singapore

⁵Physikalisches Institut, Goethe University, 60438 Frankfurt am Main, Germany

⁶Department of Physics, V. Karazin National University, 61077 Kharkiv, Ukraine

⁷National University of Science and Technology, "MISiS", Moscow 119049, Russian Federation

⁸Depto. Física de Materiales, Universidad del País Vasco, UPV/EHU, 20018 San Sebastián, Spain

⁹IKERBASQUE, The Basque Foundation for Science, 48013 Bilbao, Spain

^{a)} Author to whom correspondence should be addressed: gleb.kakazei@fc.up.pt

ABSTRACT

Magnetic skyrmions which are topologically nontrivial magnetization configurations have attracted much attention recently due to their potential applications in information recording and signal processing. Conventionally, magnetic skyrmions are stabilized by chiral bulk or interfacial Dzyaloshinskii-Moriya interaction (DMI) in noncentrosymmetric B20 bulk crystals (at low temperatures) or ultrathin magnetic films with out-of-plane magnetic anisotropy (at room temperature), respectively. The skyrmion stability in the ultrathin films relies on a delicate balance of their material parameters that are hard to control experimentally. Here, we propose an alternate approach to stabilize a skyrmion in ferromagnetic media by modifying its surroundings in order to create strong dipolar fields of the radial symmetry. We demonstrate that artificial magnetic skyrmions can be stabilized even in a simple media such as a continuous soft ferromagnetic film, provided that it is coupled to a hard magnetic antidot matrix by exchange and dipolar interactions, without any DMI. Néel skyrmions, either isolated or arranged in a 2D array with a high packing density, can be stabilized using antidot as small as 40 nm in diameter for soft magnetic films made of Permalloy. When the antidot diameter is increased, the skyrmion configuration transforms into a curled one, becoming an intermediate between the Néel and Bloch skyrmions. In addition to skyrmions, the considered nanostructure supports the formation of nontopological magnetic solitons that may be regarded as skyrmions with a reversed core.

© 2019 Author(s). All article content, except where otherwise noted, is licensed under a Creative Commons Attribution (CC BY) license (<http://creativecommons.org/licenses/by/4.0/>). <https://doi.org/10.1063/1.5093371>

I. INTRODUCTION

The development of new data storage technologies that combine ultrahigh areal density and low power consumption is one of the highest priorities of modern nanoscience. Recently, topologically stabilized magnetization configurations—magnetic skyrmions—were proposed as candidates for the implementation of the next generation of memory and logic devices.¹ Magnetic skyrmions which

are two-dimensional spin textures with sizes ranging from a few to several hundred nanometers have been the focus of interest of researchers during the last decade. Hexagonal skyrmion lattices were discovered in noncentrosymmetric crystals with B20 structure^{2–4} and in ultrathin Fe/Ir(111) films,^{5,6} at low temperatures. Then, the concept of individual skyrmion stabilization in ultrathin films at room temperature by interface induced Dzyaloshinskii-Moriya interaction (DMI) was suggested by Fert *et al.*,^{7,8} resulting in

observation of such skyrmions in ultrathin multilayer films and dots of Co/Pt, Ir/Co/Pt, etc.^{9–13} Both kinds of chiral skyrmions are stabilized due to the presence of the relativistic Dzyaloshinskii-Moriya interaction, bulk DMI^{14,15} in the former and interface DMI¹⁶ in the latter case. The main requirements for application of nanoscale skyrmions in information processing and spintronic devices are skyrmion stability at room temperature and without an external magnetic field. The lattices of B20 skyrmions are stable only at low temperatures and high magnetic fields, which makes their use in any device applications difficult.

It was found recently that magnetic skyrmions can be driven by a spin-transfer torque mechanism at a very low current density.¹⁷ This enables devices with much smaller power consumption and faster processing. The effect has been demonstrated at low temperatures in both chiral bulk magnetic structures^{18–20} and ultrathin films.^{21,22}

Recently, the controllable creation, annihilation, and manipulation of interfacial-DMI induced nanoscale skyrmions at room temperature were experimentally demonstrated.^{9–13,23} However, the room temperature skyrmion stability in the ultrathin films relies on a delicate balance of the exchange interaction, uniaxial magnetic anisotropy, and DMI. These parameters are poorly controlled for layer thicknesses of and below 1 nm. Thus, skyrmions in such films are typically metastable, i.e., they can be easily destroyed by thermal agitation or weak external fields.²⁴ Alternatively, it was demonstrated that Bloch skyrmions can be stabilized in the absence of DMI either in artificial crystals formed by the combination of nanodot arrays and perpendicularly magnetized films²⁵ or in sub-micron dots with moderate perpendicular magnetic anisotropy.^{26,27} Also, skyrmion lattices at room temperature in the absence of external magnetic field, stabilized by a competition between the intrinsic exchange, magnetocrystalline anisotropy, and dipolar interaction, were experimentally observed in a multiferroic Ni₂MnGa single crystals with inversion symmetry.²⁸ However, relatively thick (at least few nanometers) films of soft magnetic materials were never considered as a medium for skyrmion formation. Their main practical advantage is much lower magnetization damping in comparison with mentioned ultrathin multilayers (e.g., for Ni₈₀Fe₂₀, the Gilbert damping constant $\alpha \leq 0.01$) that allows us to consider microwave devices on their basis. As expected, the stabilization of skyrmions in such objects requires principally new underlying mechanisms.

In this work, by means of analytical theory and micromagnetic simulations, we demonstrate the route to obtain stable magnetic skyrmions and their dense arrays in soft ferromagnetic continuous films without DMI. Our main idea is to create skyrmions by means of a strong stray dipolar field generated by a patterned hard magnetic layer near the soft magnetic film in a hybrid bilayer structure. Recently, we have used a similar approach to overcome the limits of vortex formation in soft ferromagnetic nanodots by dipolarly coupling them to the antidot matrix.²⁹ Here, we show that the competing exchange and dipolar interactions in the patterned nanostructures can lead to the stabilization of magnetic topological soliton states, including chiral Néel and curled skyrmions, as well as their nontopological counterparts.

The nanostructure under consideration is shown in Fig. 1. It consists of a continuous soft ferromagnetic film of thickness t_{SL} , which is in contact with a patterned hard magnetic layer of

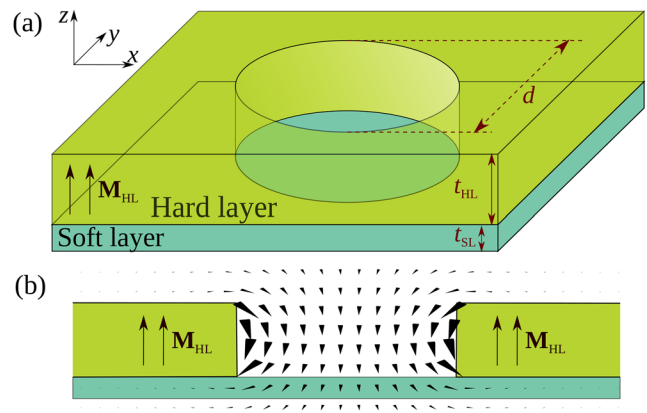


FIG. 1. (a) Schematic of the considered nanostructure, consisting of a soft magnetic layer underneath of a hard magnetic antidot matrix with perpendicular magnetization. (b) Cross section showing the distribution of the stray magnetic field created by the hard layer.

thickness t_{HL} , having a circular hole (an antidot) with diameter d . The hard layer (HL) possesses sufficient perpendicular magnetic anisotropy for the magnetization to be in the saturated out-of-plane state at zero external field. Since the soft and hard magnetic layers are in direct contact, a nonzero interlayer exchange interaction exists between them. The antidot can be isolated, or a two-dimensional antidot lattice can be formed in the film plane.

II. ANALYTICAL THEORY

A. Model and magnetic energy of the nanostructure

To understand which magnetization configurations can be stabilized in the studied nanostructure, we consider the magnetic energy of the system as a functional of its magnetic state.³⁰ We assume that the magnetization in the hard layer is uniform and is directed perpendicularly to the film plane, $\mathbf{M}_{HL} = pM_{HL}\mathbf{e}_z$, where $p = \pm 1$ corresponds to the magnetization direction “up” or “down,” M_{HL} is the saturation magnetization of the hard layer, and \mathbf{e}_z is the out-of-plane unit vector. This assumption is valid if the perpendicular magnetic anisotropy of the hard layer is sufficiently strong (see [supplementary material](#), SM #2 for details). In addition, we assume that the thickness of the soft layer is of the order of or smaller than the material exchange length so that the magnetization distribution of the soft layer can be considered uniform along the thickness z -coordinate. In the following, we consider the case of an isolated antidot.

The magnetic energy of the soft layer can be written as $W[\mathbf{M}_{SL}(\boldsymbol{\rho})] = \int w d^2\rho$, where $\boldsymbol{\rho}$ is the two-dimensional radius-vector in the soft layer plane and w is the energy density. The latter is comprised by the nonuniform exchange (w_{ex}), Zeeman (w_Z), dipolar (w_{dip}), and interlayer exchange (w_{IL}) contributions. For derivation of the explicit expressions for magnetic energy density, we describe the magnetization of the soft layer in terms of the spherical azimuthal and polar angles θ and φ so that $\mathbf{M}_{SL} = M_{SL}(\sin\theta\cos\varphi, \sin\theta\sin\varphi, \cos\theta)$. Then, the nonuniform

exchange energy is

$$w_{\text{ex}} = t_{\text{SL}} A_{\text{SL}} ((\nabla\theta)^2 + (\nabla\varphi)^2 \sin^2\theta), \quad (1)$$

where A_{SL} is the exchange stiffness of the soft layer. The energy of the interlayer exchange is equal to

$$w_{\text{IL}} = -pJ \cos\theta \Theta(\rho/R - 1), \quad (2)$$

where $\Theta(x)$ is the Heaviside step function³¹ and J is the interlayer exchange strength.

The term w_z describes the energy of the magnetization in an external magnetic field. In the considered case, the magnetic field consists of two contributions: the applied field, which is assumed to be perpendicular to the film plane ($\mathbf{B}_e = B_{e,z}\mathbf{e}_z$), and the stray field \mathbf{B}_{ad} produced by the hard layer with an antidot. The stray field is radially symmetric and has two components, perpendicular to the film plane component $B_{\text{ad},z}$ and a radial component $B_{\text{ad},\rho}$ (see [supplementary material](#), SM #1 for details). The first one is approximately constant in the soft film region under the antidot and changes its sign near the antidot border [see [Fig. 2\(a\)](#)]. The radial component increases with the distance from the antidot center and peaks at its border before decaying toward zero. Using the in-plane polar coordinate system (ρ, χ) , the Zeeman energy density is expressed as

$$w_z = -t_{\text{SL}} M_{\text{SL}} (B_z \cos\theta + B_\rho \sin\theta \cos(\varphi - \chi)). \quad (3)$$

The dipolar energy is produced by nonzero magnetostatic charges, which have two contributions—surface charges $\mathbf{M} \cdot \mathbf{e}_z$ and volume charges $(\nabla \cdot \mathbf{M})$. In thin films, the first contribution can be approximated as the energy density,

$$w_{\text{dip},s} = t_{\text{SL}} \frac{\mu_0 M_{\text{SL}}^2}{2} \cos^2\theta, \quad (4)$$

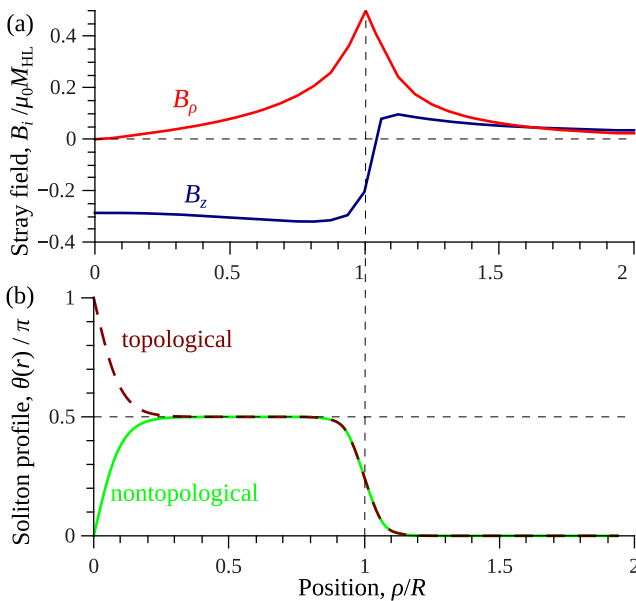


FIG. 2. (a) Normalized profile of the stray field, created by the hard magnetic layer with an antidot, in the soft magnetic one (micromagnetic calculations). The antidot aspect ratio $t_{\text{HL}}/R = 0.75$. (b) Schematic magnetization profiles of topological and nontopological solitons expected in the nanostructure.

i.e., it describes the in-plane shape anisotropy of a thin ferromagnetic film. For calculation of the volume contribution, we assume that the solution we are searching for has a radial symmetry, $\theta = \theta(\rho)$ and $\varphi(\rho, \chi) = \chi + \psi(\rho)$. This is a natural assumption because of the radial symmetry of the nanostructure. Then, the density of volume charges $\nabla \cdot \mathbf{M} = M_{\text{SL}} \rho^{-1} \partial_\rho [\rho \sin\theta(\rho) \cos\psi(\rho)]$ depends only on the radial coordinate ρ . This means that the corresponding dipolar field has only a radial component, $B_{\text{dip},\rho}(\rho) = \mu_0 \int G_{\rho\rho}(\rho, \rho') M_\rho(\rho') d^2\rho'$, where $G_{\rho\rho}$ is the $\rho\rho$ -component of the tensor magnetostatic Green's function, defined in [supplementary material](#), SM #1, averaged over the film thickness. In the case $\varphi = \chi \pm \pi/2$, the volume magnetic charges and corresponding demagnetizing field are identically equal to zero. The density of the volume contribution to the dipolar energy density is equal to

$$w_{\text{dip},v} = -t_{\text{SL}} \frac{M_{\text{SL}}}{2} \sin\theta \cos(\varphi - \chi) B_{\text{dip},\rho}. \quad (5)$$

B. Soliton structure

Stable and metastable magnetization distributions of the soft layer correspond to minima of the energy $W[\mathbf{M}_{\text{SL}}(\rho)]$. Away from the antidot, the magnetization distribution is determined by competing dipolar and interlayer exchange interactions. If the interlayer exchange energy (J) is strong enough, at least $J > t_{\text{SL}} \mu_0 M_{\text{SL}}^2$ (see details in [supplementary material](#), SM #2), the soft layer has perpendicular magnetization. It is easy to satisfy this inequality for high quality soft/hard interfaces.

Magnetization distributions that minimize the energy $W[\mathbf{M}_{\text{SL}}(\rho)]$ are the solutions of the corresponding Euler-Lagrange equation. The equation for the azimuthal magnetization angle $\varphi(\rho)$ has the following form:

$$\lambda_{\text{SL}}^2 \nabla(\sin^2\theta \nabla\varphi) = \frac{1}{\mu_0 M_{\text{SL}}} (B_\rho + B_{\text{dip},\rho}[\theta, \varphi]) \sin\theta \sin(\varphi - \chi), \quad (6)$$

where $\lambda_{\text{SL}} = \sqrt{2A_{\text{SL}}/\mu_0 M_{\text{SL}}^2}$ is the exchange length of the soft layer material ($\lambda_{\text{SL}} \approx 5$ nm for Permalloy). It is clear that Eq. (6) has exact solutions $\varphi = \chi$ or $\varphi = \chi + \pi$, which correspond to the radial direction of the in-plane magnetization component, as is in Néel skyrmion configurations. Simultaneously, it follows from Eq. (6) that the function $\varphi = \chi \pm \pi/2$ is not a solution, although in this case $B_{\text{dip},\rho}[\theta, \varphi] = 0$. Thus, we cannot expect the formation of magnetic solitons with an exact Bloch-like structure, for example, Bloch skyrmions. Instead, Eq. (6) has a solution in the form $\varphi = \chi + \psi(\rho)$, which describes a magnetization configuration with a complex curling in-plane component. The Néel-like magnetization configuration is favored by the Zeeman term (the magnetization direction is parallel to the radial stray field), while the dipolar term promotes the formation of curled magnetization distribution (to minimize the volume “magnetic charges”). Therefore, one can expect a transition from the Néel-like solitons to the curled solitons when the role of the dipolar energy increases in comparison with the Zeeman energy.

Next, we consider the properties of the function $\theta(\rho)$ in the case of Néel-like solitons with $\varphi = \chi$, which can be realized for the hard layer polarization $p = +1$ (so that the in-plane magnetization component is parallel to the radial stray field). Then, the magnetic energy density is reduced to

$$w = t_{\text{SL}} A_{\text{SL}} \left(\left(\frac{d\theta}{d\rho} \right)^2 + \left(\frac{1}{\rho^2} - \frac{1}{\lambda_{\text{SL}}^2} \right) \sin^2 \theta \right) - t_{\text{SL}} M_{\text{SL}} (B_z \cos \theta + B_\rho \sin \theta) + w_{\text{dip,v}} + w_{\text{IL}}, \quad (7)$$

where $B_\rho > 0$. Equation (7) determines the properties of the function $\theta(\rho)$, namely, $\theta(\infty) \rightarrow 0$, and $\sin \theta \cos \theta \rightarrow C\rho$, $d\theta/d\rho \rightarrow C$ at $\rho \rightarrow 0$ (see [supplementary material](#), SM #3 for details). These conditions are the same as for two-dimensional solitons in easy-axis ferromagnetic films.³² Accounting that the soliton topological charge is proportional to $\cos \theta(0) - \cos \theta(\infty)$,³⁰ the solitons can be either topological, when $\theta = \pi - C\rho$ at $\rho \rightarrow 0$, so that the magnetization direction in the core and that far from the core at $\rho \rightarrow \infty$ are opposite, or nontopological, with $\theta = C\rho$ at $\rho \rightarrow 0$. In the case when the external magnetic field almost compensates the z -component of the antidot stray field, the second term in Eq. (7) stimulates the formation of an in-plane magnetization, $\theta = \pi/2$ at $\rho > \lambda_{\text{SL}}$. Moreover, the radial component of the stray field also promotes the magnetization to lie in the soft layer plane and even leads to a decrease in the soliton core size (see [supplementary material](#), SM #4). Thus, one can expect the following structure of magnetic solitons: a core with out-of-plane magnetization in the center of the antidot followed by an in-plane magnetized part and the transition to the magnetization direction $\theta = 0$ near the antidot edge, as depicted schematically in Fig. 2(b). It should be noted that in the considered case of the compensated out-of-plane stray field, the energy of a soliton does not depend on the core polarization. Thus, both the topological soliton (skyrmion) and the nontopological soliton can exist simultaneously.

III. MICROMAGNETIC SIMULATIONS

In order to validate the analytical calculations and provide a deeper insight into possible magnetization distributions in the studied hybrid nanostructure (Fig. 1), we performed a set of micromagnetic simulations, using the MuMax3 micromagnetic simulation code.³³ We used Ni₈₀Fe₂₀ (Permalloy, saturation magnetization $M_{\text{SL}} = 8.1 \times 10^5$ A/m, exchange stiffness $A_{\text{SL}} = 1.05 \times 10^{-11}$ J/m) for the soft ferromagnetic layer, which has low damping ($\alpha \leq 0.01$) and, therefore, good microwave properties. For the material of hard layer (HL) with antidots, we have explored different materials with saturation magnetization varied from $M_{\text{HL}} = 4 \times 10^5$ A/m (Co/Pd multilayers) to $M_{\text{HL}} = 1 \times 10^6$ A/m (Fe/Pt multilayers). Our simulations showed qualitatively the same results within the studied range of the magnetic and geometrical parameters. However, higher values of the saturation magnetization of the hard layer allow for the formation of magnetic soliton configurations at smaller matrix thicknesses t_{HL} and for smaller antidot diameters d due to the stronger stray magnetic field generated by the antidot matrix. For this reason, here we focused our attention on the study of the magnetic behavior of patterned nanostructures with a hard layer of large saturation magnetization: we used the material parameters of Fe/Pt multilayers with $M_{\text{HL}} = 1000$ kA/m, exchange stiffness $A_{\text{HL}} = 2 \times 10^{-11}$ J/m, and perpendicular anisotropy constant $K_u = 1 \times 10^6$ J/m³.³⁴ The thickness of the Permalloy layer was fixed at 3 nm, while the matrix thickness, antidot diameter, and distance between them were systematically varied. The cell size was fixed to $(2 \times 2 \times 1)$ nm³. We also performed simulations with different cell sizes along the z -direction to verify that there are no simulation artifacts in the calculations of

the exchange coupling between the layers. The interlayer exchange coupling between the layers was introduced as the volume exchange interaction with the exchange stiffness being the mean value of stiffness of soft and hard layers, $A_{\text{IL}} = (A_{\text{SL}} + A_{\text{HL}})/2$. This approach is often used in micromagnetic simulations and was confirmed experimentally, i.e., for a CoPd/NiFe multilayer system.³⁵ Formally, it is equivalent to the interlayer coupling with the constant $J = (A_{\text{SL}} + A_{\text{HL}})/(a_{\text{SL}} + a_{\text{HL}}) \approx 70$ mJ/m², where a is the lattice constant of the corresponding layer. The effects of interantidot interactions were studied by the application of the periodic boundary condition with the unit cell 2×2 and 4×4 antidots.

In the simulations, a strong perpendicular external magnetic field of 1.2 T was applied first in order to completely saturate the hybrid nanostructure. After saturation, the applied magnetic field was gradually reduced to zero, and magnetization configuration was found at each step of the field decrease by the energy minimization starting from previous one (damping constants were set $\alpha_{\text{SL}} = \alpha_{\text{HL}} = 0.1$ to speed up simulations). A sufficiently large perpendicular anisotropy in the hard layer prevents matrix reversal in zero and moderate negative fields.

First, we consider the case of an isolated antidot. Different magnetization configurations of the soft layer, observed at remanence for a fixed thickness of the hard layer $t_{\text{HL}} = 20$ nm and different antidot diameters, are shown in Fig. 3. In the case of very small antidots, $d \leq 30$ nm, the remanent state is a quasi-single-domain (SL) with an almost completely in-plane magnetization in the region below the antidot [Fig. 3(a)]. When the diameter is increased, we observe different soliton magnetization configurations. In the range $d = 40$ –60 nm, the remanent state is a Néel skyrmion [Fig. 3(b)]. For $d = 75$ –150 nm, we observe the formation of a nontopological counterpart of the Néel skyrmion, which has the same direction of magnetization in the core and away from the antidot, separated by a region with in-plane magnetization pointing in a radial direction [Fig. 3(c)]. Finally, in perfect agreement with analytical predictions, the in-plane part of the magnetization distribution becomes curled with a further increase in antidot diameter and the soliton becomes an intermediate state between the Néel and Bloch solitons [Fig. 3(e)]. It is clear that the polar angle of magnetization varies with the distance from the soliton core. This is related to the spatial dependence of the radial component of the stray field generated by the antidot matrix. Note that the magnetization configuration of the soft layer is determined by the polarity of the hard layer, chosen to be $p = +1$. If it is reversed, then the magnetization of the soft layer is reversed too. In particular, the Néel skyrmion becomes of inward structure, instead of the outward one shown in Fig. 3.

Note that in the case of zero external magnetic field, the perpendicular component B_z of the stray field is not compensated. This removes the energy degeneracy of the skyrmion and its nontopological counterpart and results in an increase in the skyrmion core size and a decrease in the core size of the nontopological solitons. It happens because in the former case the core direction is parallel to the total field, while in the latter it is antiparallel [compare Figs. 3(c) and 3(d)]. In addition, the uncompensated perpendicular stray field leads to a weak tilt of the “in-plane” part of the magnetic soliton from perfect in-plane direction. Of course, when the stray field is compensated by an external field, this tilt disappears and the solitons acquire a structure shown schematically

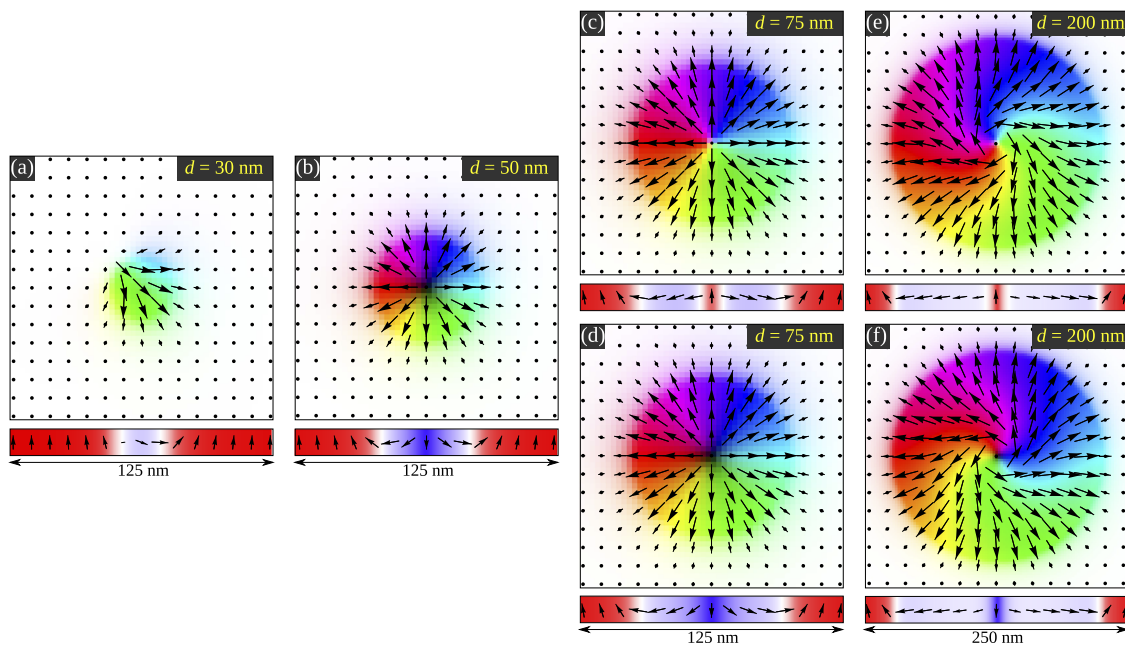


FIG. 3. Different remanent states of the soft layer in zero bias field: top—in-plane view, bottom— x - z central cross section. (a) Quasi-single-domain state (antidot diameter $d = 30$ nm). [(b) and (d)] Néel skyrmion ($d = 50$ nm and 75 nm, respectively). (c) Néel nontopological soliton ($d = 75$ nm). (e) Curled nontopological soliton ($d = 200$ nm). (f) Curled skyrmion ($d = 200$ nm). The soft film thickness is 3 nm, and the hard layer thickness is 20 nm. Note different scales for (a)–(d) and (e) and (f) correspondently.

in Fig. 2(b) with degenerated skyrmion and nontopological soliton configurations.

The observation of skyrmions or nontopological solitons at remanence is directly related with the strength of the out-of-plane stray field of the antidot matrix. This effect is clearly seen in the simulated minor hysteresis loops, shown in Fig. 4. These loops were obtained by the application of an external magnetic field, which was varied from $+1.2$ T to -0.5 T and then back to $+1.2$ T, thus avoiding the magnetization reversal of the matrix. The hysteresis loops are asymmetric with respect to the external field. This asymmetry is more pronounced for smaller antidot diameters and, naturally, for thicker hard layers. Therefore, for smaller values of the antidot diameter (e.g., for $d = 50$ nm), both core reversals, from up to down and back, occur at positive external fields. This results in the

existence of only one stable configuration at remanence, with the core polarity opposite to the matrix magnetization, i.e., skyrmion configuration [Fig. 4(a)]. On the contrary, for larger antidot diameters (e.g., for $d = 100$ nm), the core reversal from up to down occurs at a relatively small negative field [Fig. 4(b)]. Therefore, there are two stable magnetic states at remanence [Figs. 3(c) and 3(d) and Figs. 3(e) and 3(f)]. While the nontopological soliton is naturally formed when the perpendicular field is reduced to zero from positive saturation, it can be transformed into the skyrmion state by applying a small negative field. However, to transform the skyrmion back into the nontopological soliton, it is necessary to apply a large positive field.

Our results are summarized in Fig. 5 in the form of a phase diagram of the different magnetization configurations of the soft

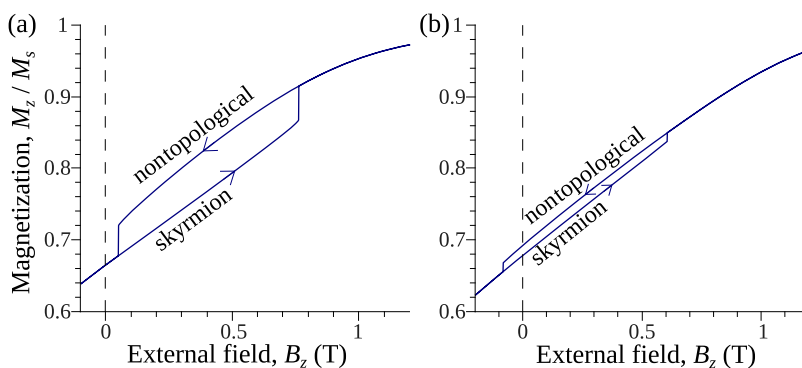


FIG. 4. Simulated minor hysteresis loop of nanostructure under a perpendicular external field (without reversal of the hard layer). For better vertical resolution, only the magnetization of the soft layer in the region twice larger in diameter than antidot is accounted. $t_{HL} = 20$ nm, $d = 50$ nm (a) and $d = 100$ nm (b).

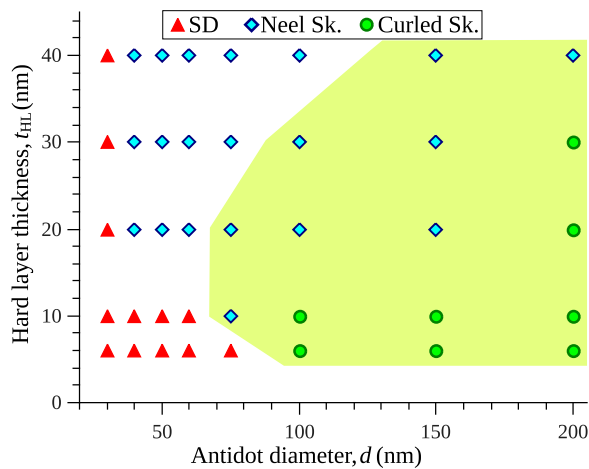


FIG. 5. Phase diagram of remanent states of the soft magnetic film after perpendicular saturation. SD—quasi-single-domain state, Sk—skyrmion. The shaded area corresponds to the region where both the skyrmion and nontopological soliton states are stable at zero bias field. Outside this region, the nontopological soliton state is unstable.

magnetic layer at remanence. The quasi-single-domain (SD) state is observed in the range of small antidots and thin hard layers. The soliton states appear at remanence above a certain critical antidot diameter for a given matrix thickness. Naturally, this critical diameter becomes smaller when the thickness of the hard layer increases since a thicker matrix creates a stronger stray field. In our simulations, we observed the Néel skyrmions in antidots as small as 40 nm in diameter. It should be emphasized that this size is much smaller than the characteristic sizes for which other topologically nontrivial configurations—magnetic vortices—are observed in isolated magnetic nanodots of the same diameter (see, e.g., Ref. 36). Thus, our simulations confirm the crucial role of the stray field generated by the antidot matrix in decreasing the soliton core size and stabilizing nontrivial magnetization configurations in smaller objects. It is clear from Fig. 5 that the Néel skyrmion is stable in the range of smaller antidot diameters and thicker hard layers. In the opposite range, the stray field from the hard matrix is smaller and the role of the demagnetizing energy of the soft layer increases, promoting the formation of curled skyrmions. The diagram also shows the region of bistability, where both skyrmion and nontopological soliton states with opposite core polarities are stable at zero field. This bistability at remanence requires larger antidots when the thickness of the hard layer increases because the perpendicular stray field from the matrix increases with the ratio t_{HL}/d increasing. Such a situation is impossible in ferromagnetic materials with bulk or interfacial Dzyaloshinskii-Moriya interaction, in which only skyrmions can be stabilized, and an attempt to reverse the skyrmion core leads to the disappearance of nontrivial magnetization configurations.

In all the simulated data presented above, the thickness of the soft layer was fixed to $t_{SL} = 3$ nm. We have performed more simulations where t_{SL} was varied. These simulations showed almost no change in the phase diagram of the remanent magnetization states (Fig. 5). This insensitivity is related to a combination of the

dominant role of the exchange interaction, the stray field from the hard layer, and dipolar contributions from surface magnetic charges in the determination of the magnetization distributions in the soft layer. All these contributions have the same dependence on the soft layer thickness [see Eqs. (2), (3), and (5)]. Only the term corresponding to the volume magnetic charges has a different dependence on the soft layer thickness [Eq. (6)]. Its effect is rather weak, especially in the determination of the critical size of the antidot supporting skyrmion formation (see supplementary material, SM #4). The only requirement on the soft layer thickness is that it should be smaller than a critical value (see calculations in supplementary material, SM #2). Above this critical value, the exchange interaction between hard and soft layers becomes insufficient to stabilize out-of-plane magnetization in the second one at positions away from the antidot. In this case, the inhomogeneous magnetization configurations exist in the soft magnetic layer, forming a kind of exchange spring.³⁷ For the studied hybrid magnetic system, it happens for Permalloy thicknesses above 5 nm.

Finally, the influence of the antidot periodicity on the soliton configuration was studied by varying the distance between antidots arranged into square arrays. For this purpose, we fixed $t_{HL} = 30$ nm and $d = 40$ nm, which is the smallest antidot diameter and hard layer thickness combination allowing the existence of the skyrmions, and vary the antidot periodicity from almost the isolated case to a very closely packed array of 60 nm periodicity. Figure 6 shows the evolution of magnetic configuration at the remanent state for different antidot periods. The Néel skyrmion for the antidot arrays with period ≥ 100 nm and the Néel nontopological soliton for the period in the range 70–90 nm can be seen in Figs. 6(a) and 6(b), respectively. Finally, at periods of 60 nm and below, the in-plane quasi-single-domain state is formed, as seen in Fig. 6(c). The decrease in antidot lattice period affects the soft magnetic layer configuration stability in a way similar as does the decrease in the hard layer thickness. Both changes lead to the reduction of the stray field density inside the antidot. However, in a broad region of the antidot lattice periods, only the polarity of the soliton is affected by a decrease in the perpendicular stray field. At very high packing densities, the radial stray field becomes weak enough to support the formation of magnetic soliton states. For antidot lattices of other geometries (e.g., honeycomb), we expect similar results since the main impact is produced by a reduction of stray fields and not by interaction (either exchange or dipolar) between neighbor solitons. Indeed, contribution from the exchange interaction is negligible since the nearest solitons are separated by uniformly magnetized regions with the size much larger than the exchange length. Also, the dipolar interaction between soliton cores decreases rapidly with the intercore distance and for the 3 nm thick core became insignificant at few tens of nanometers.^{38–40} Therefore, the only difference between various lattice geometries will be in the critical lattice constant at which the skyrmion state loses its stability. The mentioned weakness of intersoliton interaction leads to the possibility to switch the magnetic configuration of individual elements in a dense square array (period 70–90 nm) from the Néel nontopological soliton to the Néel skyrmion by applying locally the relatively small negative perpendicular field. This property allows us to consider the proposed system for applications in information storage as recording media and in magnonics as reconfigurable two-dimensional magnonic crystals.⁴¹

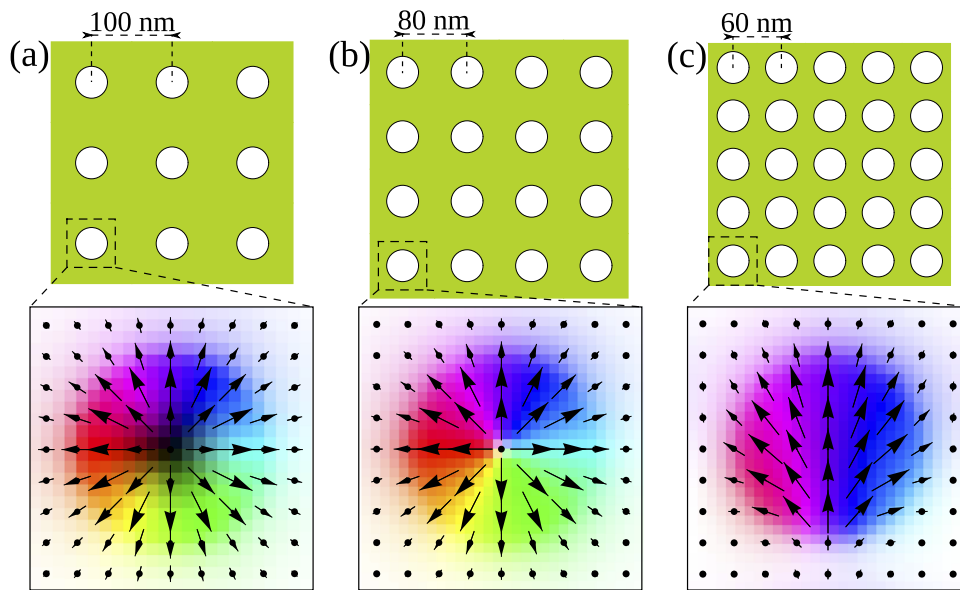


FIG. 6. Remanent magnetization states of the soft magnetic film, coupled to a 30 nm thick antidot matrix with antidots of diameter 40 nm and different periods of the square antidot lattice: (a) 100 nm antidot lattice period (Néel skyrmion state), (b) 80 nm period (Néel nontopological state), (c) 60 nm period (quasi-single-domain state).

IV. CONCLUSIONS

We have demonstrated a novel method to achieve magnetic skyrmion configurations in soft ferromagnetic films without Dzyaloshinskii-Moriya interaction. Our approach is based on using a hybrid nanostructure, where a soft magnetic layer is coupled by dipolar and interlayer exchange interactions to an out-of-plane magnetized hard layer having an antidot or antidot lattice. In this nanostructure, interlayer exchange is responsible for the soft layer magnetization direction away from the antidot (out-of-plane direction). Simultaneously, the radial component of the stray magnetic field generated by the antidot plays a crucial role in the formation of inhomogeneous magnetization configurations in the soft magnetic layer near the antidot—the radial Néel skyrmions.

We showed by means of micromagnetic simulations that the proposed patterned nanostructure allows for the realization of topologically nontrivial magnetization configurations for antidots as small as 40 nm in diameter (for a Permalloy soft magnetic layer). Depending on the material and geometric parameters, it is possible to achieve the formation of stable Néel solitons (skyrmions or their nontopological counterparts) at remanence, or curled solitons with a complex magnetization distribution, resembling an intermediate state between the Néel and Bloch skyrmions. The formation of the curled solitons is a result of the competing demagnetizing and Zeeman energy contributions to the stray field created by the antidot matrix. The curled skyrmions are realized in the case of relatively thin hard layers and large antidot diameters, while smaller antidots and thicker hard layers support the formation of Néel skyrmions.

The proposed nanostructure also allows for the formation of a two-dimensional skyrmion lattice with a high packing density. When the separation between antidots becomes smaller than their sizes, the skyrmion configuration in the soft layer is suppressed in favor of a quasi-single-domain state. Our findings open a way

for investigation of the magnetic skyrmions in soft magnetic materials with good high-frequency properties due to low magnetization damping and their possible applications in microwave and information storage devices.

SUPPLEMENTARY MATERIAL

See [supplementary material](#) for different aspects of analytical theory that are described in detail: calculation of the stray field from a hard magnetic layer with an antidot (SM #1), condition on the interlayer exchange (SM #2), properties of the function $\theta(\rho)$ determining the magnetization profile of the soft magnetic layer (SM #3), and estimation of the soliton core radius (SM #4).

ACKNOWLEDGMENTS

The Portuguese team acknowledges the Network of Extreme Conditions Laboratories-NECL and Portuguese Foundation of Science and Technology (FCT) support through Project Nos. NORTE-01-0145-FEDER-022096, MIT-EXPL/IRA/0012/2017, POCI-0145-FEDER-030085 (NOVAMAG), PTDC/FIS-MAC/31302/2017, EXPL/IF/00541/2015 (S.A.B.), and Grant No. SFRH/BPD/90471/2012 (A.H.-R.). Work at IMag was supported by the Ministry of Education and Science of Ukraine (Project No. 0118U004007). K.Y.G. acknowledges support from IKERBASQUE (the Basque Foundation for Science) and the Spanish MINECO, Grant No. FIS2016-78591-C3-3-R. R.V.V. B.A.I., K.Y.G., and O.V.D. acknowledge the support from the European Union Horizon 2020 Research and Innovation Programme under Marie Skłodowska-Curie, Grant Agreement No. 644348. A.H.-R. acknowledges the support from Spanish MINECO under Project Ref. No. FIS2016-76058-C4-4-R and from European Union's Horizon 2020 research and innovation program under the Marie Skłodowska-Curie Action Reference No. H2020-MSCA-IF-2016-746958. B.A.I. was supported by the Program of NUST "MISiS" (Grant No. K2-2017-005), implemented

by a governmental decree dated 16th of March 2013, No. 211. G.N.K. and O.V.D. acknowledge the support from European Cooperation in Science and Technology (COST), Project No. CA16218 “NANOCO-HYBRI”. A.O.A. was supported by the Ministry of Education, Singapore, under Research Project No. R-263-000-C61-112. A.O.A. is a member of Singapore Spintronics Consortium (SG-SPIN).

REFERENCES

- ¹A. Fert, N. Reyren, and V. Cros, *Nat. Rev. Mater.* **2**, 17031 (2017).
- ²S. Muhlbauer, B. Binz, F. Jonietz, C. Pfleiderer, A. Rosch, A. Neubauer, R. Georgii, and P. Boni, *Science* **323**, 915 (2009).
- ³X. Z. Yu, Y. Onose, N. Kanazawa, J. H. Park, J. H. Han, Y. Matsui, N. Nagaosa, and Y. Tokura, *Nature* **465**, 901 (2010).
- ⁴X. Z. Yu, N. Kanazawa, Y. Onose, K. Kimoto, W. Z. Zhang, S. Ishiwata, Y. Matsui, and Y. Tokura, *Nat. Mater.* **10**, 106 (2011).
- ⁵S. Heinze, K. von Bergmann, M. Menzel, J. Brede, A. Kubetzka, R. Wiesendanger, G. Bihlmayer, and S. Blügel, *Nat. Phys.* **7**, 713 (2011).
- ⁶N. Romming, C. Hanneken, M. Menzel, J. E. Bickel, B. Wolter, K. von Bergmann, A. Kubetzka, and R. Wiesendanger, *Science* **341**, 636 (2013).
- ⁷A. Fert, V. Cros, and J. Sampaio, *Nat. Nanotechnol.* **8**, 152 (2013).
- ⁸J. Sampaio, V. Cros, S. Rohart, A. Thiaville, and A. Fert, *Nat. Nanotechnol.* **8**, 839 (2013).
- ⁹C. Moreau-Luchaire, C. Moutafis, N. Reyren, J. Sampaio, C. A. F. Vaz, N. Van Horne, K. Bouzehouane, K. Garcia, C. Deranlot, P. Warnicke, P. Wohlhüter, J.-M. George, M. Weigand, J. Raabe, V. Cros, and A. Fert, *Nat. Nanotechnol.* **11**, 444 (2016).
- ¹⁰O. Boulle, J. Vogel, H. Yang, S. Pizzini, D. de Souza Chaves, A. Locatelli, T. O. Menteş, A. Sala, L. D. Buda-Prejbeanu, O. Klein, M. Belmeguenai, Y. Roussigné, A. Stashkevich, S. M. Chérif, L. Aballe, M. Foerster, M. Chshiev, S. Auffret, I. M. Miron, and G. Gaudin, *Nat. Nanotechnol.* **11**, 449 (2016).
- ¹¹S. Woo, K. Litzius, B. Krüger, M.-Y. Im, L. Caretta, K. Richter, M. Mann, A. Krone, R. M. Reeve, M. Weigand, P. Agrawal, I. Limesh, M.-A. Mawass, P. Fischer, M. Kläui, and G. S. D. Beach, *Nat. Mater.* **15**, 501 (2016).
- ¹²S. D. Pollard, J. A. Garlow, J. Yu, Z. Wang, Y. Zhu, and H. Yang, *Nat. Commun.* **8**, 14761 (2017).
- ¹³W. Jiang, P. Upadhyaya, W. Zhang, G. Yu, M. B. Jungfleisch, F. Y. Fradin, J. E. Pearson, Y. Tserkovnyak, K. L. Wang, O. Heinonen, S. G. E. te Velthuis, and A. Hoffmann, *Science* **349**, 283 (2015).
- ¹⁴A. N. Bogdanov and D. A. Yablonskii, *Sov. Phys. JETP* **95**, 178 (1989).
- ¹⁵B. A. Ivanov, V. A. Stephanovich, and A. A. Zhmudskii, *J. Magn. Magn. Mater.* **88**, 116 (1990).
- ¹⁶H. Yang, A. Thiaville, S. Rohart, A. Fert, and M. Chshiev, *Phys. Rev. Lett.* **115**, 267210 (2015).
- ¹⁷N. Locatelli, V. Cros, and J. Grollier, *Nat. Mater.* **13**, 11 (2014).
- ¹⁸L. Liu, C.-T. Chen, and J. Z. Sun, *Nat. Phys.* **10**, 561 (2014).
- ¹⁹X. Z. Yu, N. Kanazawa, W. Z. Zhang, T. Nagai, T. Hara, K. Kimoto, Y. Matsui, Y. Onose, and Y. Tokura, *Nat. Commun.* **3**, 988 (2012).
- ²⁰F. Jonietz, S. Muhlbauer, C. Pfleiderer, A. Neubauer, W. Munzer, A. Bauer, T. Adams, R. Georgii, P. Boni, R. A. Duine, K. Everschor, M. Garst, and A. Rosch, *Science* **330**, 1648 (2010).
- ²¹J. Iwasaki, M. Mochizuki, and N. Nagaosa, *Nat. Nanotechnol.* **8**, 742 (2013).
- ²²K. Litzius, I. Limesh, B. Krüger, P. Bassirian, L. Caretta, K. Richter, F. Büttner, K. Sato, O. A. Tretiakov, J. Förster, R. M. Reeve, M. Weigand, I. Bykova, H. Stoll, G. Schütz, G. S. D. Beach, and M. Kläui, *Nat. Phys.* **13**, 170 (2017).
- ²³F. Büttner, C. Moutafis, M. Schneider, B. Krüger, C. M. Günther, J. Geilhufe, C. v. K. Schmising, J. Mohanty, B. Pfau, S. Schaffert, A. Bisig, M. Foerster, T. Schulz, C. A. F. Vaz, J. H. Franken, H. J. M. Swagten, M. Kläui, and S. Eisebitt, *Nat. Phys.* **11**, 225 (2015).
- ²⁴R. Tomasello, K. Y. Guslienko, M. Ricci, A. Giordano, J. Barker, M. Carpentieri, O. Chubykalo-Fesenko, and G. Finocchio, *Phys. Rev. B* **97**, 060402 (2018).
- ²⁵L. Sun, R. X. Cao, B. F. Miao, Z. Feng, B. You, D. Wu, W. Zhang, A. Hu, and H. F. Ding, *Phys. Rev. Lett.* **110**, 167201 (2013).
- ²⁶K. Y. Guslienko, *IEEE Magn. Lett.* **6**, 4000104 (2015).
- ²⁷M. Zelent, J. Tóbiš, M. Krawczyk, K. Y. Guslienko, and M. Mruczkiewicz, *Phys. Status Solidi - Rapid Res. Lett.* **11**, 1700259 (2017).
- ²⁸C. Phatak, O. Heinonen, M. De Graef, and A. Petford-Long, *Nano Lett.* **16**, 4141 (2016).
- ²⁹R. V. Verba, D. Navas, A. Hierro-Rodriguez, S. A. Bunyaev, B. A. Ivanov, K. Y. Guslienko, and G. N. Kakazei, *Phys. Rev. Appl.* **10**, 031002 (2018).
- ³⁰A. M. Kosevich, B. A. Ivanov, and A. S. Kovalev, *Phys. Rep.* **194**, 117 (1990).
- ³¹G. B. Arfken and H. J. Weber, *Mathematical Methods for Physicists* (Academic Press, New York, 1995).
- ³²A. S. Kovalev, A. M. Kosevich, and K. V. Maslov, *JETP Lett.* **30**, 296 (1979).
- ³³A. Vansteenkiste, J. Leliaert, M. Dvornik, M. Helsen, F. Garcia-Sanchez, and B. Van Waeyenberge, *AIP Adv.* **4**, 107133 (2014).
- ³⁴R. F. C. Farrow, D. Weller, R. F. Marks, M. F. Toney, D. J. Smith, and M. R. McCartney, *J. Appl. Phys.* **84**, 934 (1998).
- ³⁵S. Tacchi, T. N. A. Nguyen, G. Carlotti, G. Gubbiotti, M. Madami, R. K. Dumas, J. W. Lau, J. Åkerman, A. Rettori, and M. G. Pini, *Phys. Rev. B* **87**, 144426 (2013).
- ³⁶K. L. Metlov and K. Y. Guslienko, *J. Magn. Magn. Mater.* **242-245**, 1015 (2002).
- ³⁷F. Garcia-Sanchez, O. Chubykalo-Fesenko, O. Mryasov, R. W. Chantrell, and K. Y. Guslienko, *Appl. Phys. Lett.* **87**, 122501 (2005).
- ³⁸J. Shibata and Y. Otani, *Phys. Rev. B* **70**, 012404 (2004).
- ³⁹K. S. Buchanan, P. E. Roy, M. Grimsditch, F. Y. Fradin, K. Y. Guslienko, S. D. Bader, and V. Novosad, *Nat. Phys.* **1**, 172 (2005).
- ⁴⁰S. S. Cherepov, B. C. Koop, A. Yu. Galkin, R. S. Khymyn, B. A. Ivanov, D. C. Worledge, and V. Korenivski, *Phys. Rev. Lett.* **109**, 097204 (2012).
- ⁴¹M. Krawczyk and D. Grundler, *J. Phys.: Condens. Matter* **26**, 123202 (2014).